Effect of Slag Composition on Dephosphorization and Foamability in the Electric Arc Furnace Steelmaking Process: Improvement of Plant Operation

JUNG HO HEO and JOO HYUN PARK

The effect of slag composition under M'O (monoxide, M = Fe,Mg) saturation and fully liquid conditions on dephosphorization and slag foamability was evaluated in an electric arc furnace (EAF) steelmaking plant operation by considering thermodynamics and phase equilibria. It was confirmed that M'O saturation slag is more favorable for higher dephosphorization than fully liquid slag due to its high activity of CaO as a thermodynamic driving force. As a quantitative measure of slag foamability, the foaming index was clearly dependent on the temperature and slag composition. Moreover, foam stability was evaluated by applying the predominance stability diagram based on phase equilibria. Consequently, it can be suggested that an efficient direction for dephosphorization and slag foaming during the EAF process is to generate high CaO activity as well as small amounts of M'O monoxide and dicalcium silicate (Ca_2SiO_4) compounds.

https://doi.org/10.1007/s11663-021-02322-3

I. INTRODUCTION

THE electric arc furnace (EAF) has evolved into a fast and low-cost melter of scrap where the major criterion is higher productivity in order to reduce fixed costs.[1] Various technologies to achieve higher production rates include oxy-fuel burners, oxygen lancing, additive injection (carbon, lime, dolomite, *etc.*), foamy slag practices, CO gas post-combustion, EAF bath stirring, and the use of an alternative iron source (*e.g.*, direct reduced iron, DRI). In particular, the desirable addition of fluxing agents and foamy slag practices, which are very important for the refining efficiency of molten steel and its productivity during EAF operation, are strongly related to the slag composition.[2–6]

Because a classic impurity in molten steel is phosphorus, the removal of phosphorus in molten steel by EAF slag is obligatorily performed during EAF operation.[7] Burnt lime (CaO) or dolomite (CaO·MgO) are used as typical fluxing agents and have high refining ability and low cost. Thus, the thermodynamics of dephosphorization of molten steel *via* CaO-based slags has been widely investigated.[5–21] However, high amounts of burnt lime and/or dolomite have been overcharged in the commercial EAF process to obtain highly basic slag, which is undesirable from a practical point of view considering the slag volume and its post-mortem treatment. A reasonable technique to achieve a higher dephosphorization efficiency is to control the content of other oxides such as Al_2O_3, Fe_tO, and MnO accompanied with high CaO activity in EAF slag. Because the thermodynamic behaviors of these amphoteric oxides, which act as an acidic or basic oxide, are dependent on the slag composition at a given oxygen potential and temperature, researches on the effect of these oxides upon dephosphorization have been widely investigated.[8,9,15–20]

In addition, the slag composition is also one of the dominant factors for promoting foamy slag because the FeO activity as a thermodynamic driving force for FeO reduction (*i.e.*, CO evolution), MgO solubility, and thermophysical properties of slags are strongly dependent on the slag composition to sustain the CO gas production reaction.[1,22–30] Specifically, the precipitation of solid compounds such as magnesiowüstite, *i.e.*, (Mg,Fe)O monoxide, and dicalcium silicate (Ca_2SiO_4, C_2S) in EAF slag directly affects slag foaming phenomena by changing the apparent viscosity of slag.[23,24] Namely, the precipitation of solid compounds

JUNG HO HEO is with the Department of Materials Science and Chemical Engineering, Hanyang University, Ansan 15588, Korea and also with the Department of Materials Engineering, KU Leuven, Kasteelpark Arenberg 44, Leuven 3001, Belgium. JOO HYUN PARK is with the Department of Materials Science and Chemical Engineering, Hanyang University. Contact e-mail: basicity@hanyang.ac.kr

Manuscript submitted April 13, 2021; accepted September 5, 2021. Article published online September 30, 2021.

significantly increases the foam stability. To precipitate (Mg,Fe)O monoxide, FeO produced by the oxidation of molten steel should react with MgO which mostly originates from dolomite and/or MgO refractory. However, because chemical corrosion of MgO refractory should be suppressed to prolong the lining life, control of the MgO content by suitably adding dolomite (not over charging) is a reasonable practice. Additionally, it was reported that the formation of a (Mg,Fe)O intermediate layer at the slag/refractory interface can improve the life of the refractory line by preventing direct corrosion of refractory by molten slag.[31,32] Thus, the formation of (Mg,Fe)O monoxide helps to increase foam stability which reduces refractory consumption.[1]

One of the roles of CaO in slag in addition to increasing the phosphate capacity is to decrease MgO solubility. It was reported that the MgO solubility decreases with increasing CaO/SiO_2 ratio, indicating that precipitation of the (Mg,Fe)O monoxide can be easily induced with small amounts of dolomite addition at a high CaO/SiO_2 ratio.[22,33] Foamability is also dependent on the CaO/SiO_2 ratio. However, an excessive increase of CaO content beyond the C_2S saturation limit is exceptionable. High amounts of C_2S in slag inordinately increase the slag viscosity, contributing to lower foam stability.[26] Thus, appropriate control of the CaO/SiO_2 ratio is very crucial to stabilize slag foam during the EAF process.

The (Mg,Fe)O monoxide and C_2S compounds suspended slag mentioned above are frequently occurred in commercial EAF plant operation due to the heterogeneous slag composition, temperature fluctuations, and impurities in the fluxing agents. The solid + liquid multiphase slag affects the foamability and dephosphorization efficiency. Even though slag foam is relatively stable in the multiphase composition region, it is estimated that the absolute quantity of phosphorus absorption by slag is inversely proportional to the solid fraction of slag. Namely, the dephosphorization efficiency is generally improved with an increase of the liquid fraction of slag. However, fully liquid slag has several practical disadvantages such as damage of refractory lines and delicate slag foaming practice. Thus, the process requires the use of small amounts of solid-containing multiphase slag, which may decrease the dephosphorization efficiency during the refining stage. However, it cannot be simply guaranteed that dephosphorization will decrease in the multiphase slag because dephosphorization is strongly affected by the basicity (*i.e.*, $a_{O^{2-}}$) of liquid slag. In addition, the thermodynamic driving force in liquid slag will change depending on which solid phases are precipitated.

In summary, a number of previous studies have investigated the effect of slag composition on dephosphorization and they generally emphasize the importance of a higher slag basicity. Because slag may be generally in a solid + liquid multiphase condition during the commercial EAF process, proper amounts of solid phases like (Mg,Fe)O monoxide and C_2S compound should be controlled by considering the phase equilibria of the slag, which affects the dephosphorization driving force as well as efficient slag foamability.

Therefore, it is necessary not only to evaluate the effect of solid + liquid multiphase slag on dephosphorization by considering the actual EAF slag operation window, but also to determine which factor mainly contributes to the increase of dephosphorization efficiency. At the same time, the foaming index should be discussed as a quantitative measure of slag foamability with interpretation based on phase equilibria. Here, the important point is to use slag composition obtained from an industrial EAF operation for the effect of solid + liquid multiphase slag on slag foaming as well as dephosphorization behavior, which is of prime importance in plant operation. Therefore, the evaluation of the dephosphorization thermodynamics and foamability of the multiphase slag will be simultaneously discussed and compared to fully liquid slag operation.

II. OPERATION OF THE ELECTRIC ARC FURNACE PROCESS

An industrial plant trial was performed in a commercial EAF melt shop in Korea. An EAF with a 70 or 140 ton nominal capacity was evaluated. The fluxing materials such as dolomite (CaO·MgO), burnt lime (CaO), and reducing agents such as carbon in a lumpy form with scrap were charged in two or three baskets during the melting stage. After melt down confirmation, pulverized coal (80 to 85 pct carbon) and Al dross (mixture of metallic Al and Al_2O_3, 20 to 25 pct metallic Al) were injected to increase the yield of steel and to induce slag foaming, which is originated by the production of CO (and CO_2) gas by carbothermic reduction. Sustainability of slag foaming is strongly dependent on slag composition and temperature. In addition, powder lime was also injected into the slag phase to refine the molten steel. Lime injection will induce transient change of slag composition and temperature during EAF refining operation. Even though temperature slightly decreases by the addition of lime, transient change of slag composition and temperature will affect the refining ability of molten slag. Furthermore, it is instantaneously possible to precipitate M'O and Ca_2SiO_4 phases by heterogeneity and local fluctuation of temperature in the furnace. High CaO (and MgO) content in slag will be able to retard MgO refractory corrosion by increasing the chemical potential of MgO in slag phase.

The entire operation time was generally about 60 minutes and the average temperature was 1843 K (1570 °C). After the required operations were completed, sampling of molten steel and slag was carefully performed before tapping. Long steel tube was used to collect metal sample, which is cylindrical in shape with about 20 mm diameter and 60 mm height, followed by air cooling. Similarly, a steel bar was immersed into

molten slag layer and then slag sample can be collected by coating the bar surrounded. Metal and slag samples were carefully detached from sampling tools and were sent for chemical analysis. The compositions of the steel and slag samples were determined by inductively coupled plasma-atomic emission spectroscopy (ICP-AES) and X-ray fluorescence spectroscopy (XRF), respectively. More details of the sampling process are available elsewhere.[22]

In this study, the slag composition is mainly divided into two conditions: fully liquid slag and monoxide (M'O) saturation slag, which were evaluated by using the phase diagram module in FactSage^{TM} 7.3 software. The average steel and slag compositions in 66 operation heats for fully liquid slag and 15 operation heats for M'O saturation slag used in this study are listed in Table I. The compositions of the two types of slag, the CaO–SiO_2–FeO-8 pct MgO-15 pct Al_2O_3-10 pct MnO system (Figure 1(a)) and the CaO–SiO_2–FeO-11 pct MgO-8 pct Al_2O_3-11 pct MnO system (Figure 1(b)), are shown in the phase diagrams in the temperature range from 1823 K to 1923 K (1550 °C to 1650 °C) and at $p(O_2) = 10^{-10}$ atm in addition to the univariant phase equilibria. The yellow region represents the liquid region at 1843 K (1570 °C).

It is noteworthy that the basicity defined as the CaO/(SiO_2 + Al_2O_3) {= C/(S + A)} ratio in M'O saturation slag (Type B: C/(S + A) = 1.12 ± 0.1) is slightly higher than in the fully liquid slag (Type A: C/(S + A) = 0.75 ± 0.09) and the Al_2O_3 content in the M'O saturation slag (Type B: Al_2O_3 = 8.4 mass pct) is about 2 times lower than in the fully liquid slag (Type A: Al_2O_3 = 15.7 mass pct). Dephosphorization and slag foaming behavior are greatly affected by changes of the slag composition, contributing to a variation of basicity and viscosity as the representative thermodynamic driving force and thermophysical property, respectively. Therefore, it is necessary to understand the fundamental thermodynamic behavior of FeO and P_2O_5, which will be discussed in Section III–A. In addition, assessment of the foaming behavior is also required based on phase equilibria, which will be discussed in Section III–B.

III. RESULTS AND DISCUSSION

A. *Influence of Basicity on the Thermodynamic Behavior of FeO and P_2O_5 Under M'O Saturation and Fully Liquid Slag Conditions*

The effect of basicity, defined as the CaO/(SiO_2 + Al_2O_3) mass ratio, on the contents of FeO and P_2O_5 in M'O saturation and fully liquid slag is shown in Figure 2. All of the slag composition data under M'O saturation are plotted along with the fully liquid slag data. The FeO content decreases with increasing basicity index with some scatters (Figure 2(a)) and the content of P_2O_5 continuously increases with increasing basicity, irrespective of the slag conditions (Figure 2(b)), *viz*. fully liquid slag and M'O saturation slag. The average P_2O_5 content in M'O saturation slag (= 0.4 ± 0.06 mass pct) is relatively higher than the one in fully liquid slag (= 0.2 ± 0.06 mass pct). The average content of FeO in M'O saturation slag (= 17.0 ± 3.9 mass pct) is relatively lower than the one in fully liquid slag (= 24.6 ± 4.1 mass pct).

The behavior of FeO and P_2O_5 in EAF slag can be thermodynamically understood by considering the activity coefficients of FeO and P_2O_5, which vary with basicity, as shown in Figure 3. The activity coefficient of FeO (γ_{FeO}) qualitatively exhibits a maximum at a basicity of about C/(S + A) = 1.0 ± 0.1, and γ_{FeO} in M'O saturation slag is higher than that in fully liquid slag. The activity coefficient of P_2O_5 ($log\gamma_{P_2O_5}$) continuously decreases with increasing basicity. In particular, $log\gamma_{P_2O_5}$ in M'O saturation slag is clearly lower than that in fully liquid slag. Namely, the stabilities of FeO and P_2O_5 are strongly dependent on the change of basicity as a thermodynamic driving force.

To quantitatively evaluate phosphorus removal during the EAF process, the effect of basicity on the distribution ratio of phosphorus ($L_P = (pct\,P_2O_5)/[pct\,P]$) for M'O saturation slag and fully liquid slag composition was evaluated, as shown in Figure 4. L_P clearly increases with increasing basicity and the average L_P value of M'O saturation slag ($L_P = 23.9$) is about 2.5 times higher than the average value of fully liquid slag ($L_P = 9.4$).

Previous results generally reported that the CaO activity in CaO-based slag is key parameter to increase the dephosphorization efficiency. CaO, which behaves as a representative basic oxide, improves the activity of free oxygen ions ($a_{O^{2-}}$) as a basicity index in molten EAF slag based on Eqs. [1] and [2].[3,34–37]

$$(CaO) = \left(Ca^{2+}\right) + \left(O^{2-}\right) \quad [1]$$

$$a_{O^{2-}} = \frac{K_{[1]} \cdot a_{CaO}}{a_{Ca^{2+}}} \quad [2]$$

Because the activity of free oxygen ions cannot be directly measured due to thermodynamic constraints, dephosphorization was indirectly evaluated by considering the CaO activity at a constant temperature by assuming that $a_{O^{2-}} \approx a_{CaO}$. Hence, the linear relationship between the logarithmic of the CaO activity and the phosphate capacity, which is expressed in Eq. [4] based on the dephosphorization reaction shown in Eq. [3], can be deduced to Eq. [5].

$$\frac{1}{2}P_2(g) + \frac{3}{2}\left(O^{2-}\right) + \frac{5}{4}O_2(g) = \left(PO_4^{3-}\right) \quad [3]$$

$$C_{PO_4^{3-}} = \frac{K_{[3]} \cdot a_{O^{2-}}^{3/2}}{f_{PO_4^{3-}}} = \frac{(\text{pct } PO_4^{3-})}{p_{P_2}^{1/2} \cdot p_{O_2}^{5/4}} \quad [4]$$

$$\log C_{PO_4^{3-}} = \frac{3}{2}\log a_{CaO} - \frac{3}{2}\log a_{Ca^{2+}} - \log f_{PO_4^{3-}} + \text{Const.}, \quad [5]$$

where $K_{[3]}$ is the equilibrium constant of Eq. [3], $a_{O^{2-}}$ is the activity of free O^{2-} ions, $f_{PO_4^{3-}}$ is the activity coefficient of phosphate ions in the slag, and $p_{i(=P_2,O_2)}$ is the partial pressure of the gaseous constituent of i (atm). The partial pressure of phosphorus gas can be obtained based on thermodynamic equilibrium reaction as follows:

$$\begin{aligned} &\frac{1}{2}P_2(g) = [P]_{inFe}, \\ &\Delta G^{\circ}_{[6]} = -157,700 + 5.4T(\text{J/mol}) \end{aligned} \quad [6]$$

$$K_{[6]} = \frac{f_P \cdot [\text{pct P}]}{p_{P_2}^{0.5}}. \quad [7]$$

Here, the activity coefficient of phosphorus (f_P) in molten steel was calculated from Eq. [8] by applying the interaction parameters between Si, Mn, P, and C listed in Table II.[38]

$$\log f_P = \sum^{i=Si,Mn,P,C} e_P^i \cdot [\text{mass pct } i] \quad [8]$$

In addition, to calculate oxygen partial pressure, the following equilibrium reaction was considered.[39]

$$\begin{aligned} Fe(l) + \frac{1}{2}O_2(g) &= (FeO), \Delta G^{\circ}_{[9]} \\ &= -256,000 + 53.7T(\text{J/mol}) \end{aligned} \quad [9]$$

$$K_{[9]} = \frac{a_{FeO}}{p_{O_2}^{0.5}}. \quad [10]$$

Here, the activity of FeO (a_{FeO}) can be obtained by using FactSage™ 7.3 software.

Based on Eq. [5], $\log C_{PO_4^{3-}}$ and $\log a_{CaO}$ indicate a linear relationship with a slope of 3/2, assuming that the compositional dependency of $a_{Ca^{2+}}$ and $f_{PO_4^{3-}}$ are not critical at a fixed temperature. A slope of about 2.0(± 0.1) was experimentally obtained from the least square regression analysis between $\log C_{PO_4^{3-}}$ and $\log a_{CaO}$, as shown in Figure 5. The slope is slightly larger than the theoretical slope (= 1.5), qualitatively indicating that the decreasing rate of $f_{PO_4^{3-}}$ is higher than the increasing rate of $a_{Ca^{2+}}$ with increasing CaO activity. Even though the slope from the relationship between $\log C_{PO_4^{3-}}$ and $\log a_{CaO}$ is slightly higher than the theoretical value, a linearity with a slope of 2.0 is reasonable within experimental scatters of plant data. This indicates that the CaO activity strongly affects dephosphorization, although the liquid fraction of slag containing a small amount of the M'O solid phase is relatively smaller than that of fully liquid slag. In other words, increasing CaO activity in liquid slag as a thermodynamic driving force is crucial to increase dephosphorization efficiency even under M'O saturation conditions.

The quantitative understanding of phosphate capacity can be more corroborated by employing the activity of each slag component. Hence, iso-activity contours of each oxide are displayed in the $CaO–SiO_2–FeO–11MgO–8Al_2O_3–11MnO$ phase diagram at 1843 K (1570 °C) in Figure 6. In particular, the activity contours of each oxide are exhibited in the liquid slag (L) region as well as the M'O saturation (L + M'O) region to compare between fully liquid and M'O saturation conditions. The CaO activity in the M'O saturation region is higher than in the fully liquid region and the SiO_2 activity in the M'O saturation region is lower than in the fully liquid region. The CaO activity dominantly affects the driving force for the dephosphorization reaction. Meanwhile, the FeO activity shows a curved response, *i.e.*, amphoteric behavior, with increasing CaO/SiO_2 ratio at a fixed FeO content.

In addition, the variation of (pct Fe/pct Mg) in the M'O phase represented as a gradation of color is observed in the L + M'O region. For better understanding, the iso-(pct Fe/pct Mg) contours are also shown in the M'O phase region from 0.3 to 2.0. In the type B slag, (pct Fe/pct Mg) in the M'O phase is a low value from around 0.3 to 1.0, indicating that the effect of MgO in slag on the chemical potential of M'O formation was more dominant than FeO in the slag. It can be estimated that protection of the MgO refractory by slag attack was quite efficient due to the low solubility of MgO in slag. However, if the value of (pct Fe/pct Mg) is high, the main source for forming the M'O phase is FeO in slag, which originates from molten steel, *i.e.*, with a lower yield of steel. Hence, (pct Fe/pct Mg) in the M'O phase may be a qualitative indicator for adequacy of the MgO content in slag and the yield of steel.

It is noteworthy that the direction of controlling slag composition from the fully liquid region to the M'O saturation region is thermodynamically efficient to increase dephosphorization based on the activity variation. However, an excessive amount of the M'O phase will apparently increase the slag viscosity, which affects the slag foaming practice. Thus, it is necessary to evaluate the effect of slag composition on slag foaming, which will be discussed in the following section.

B. *Influence of Slag Composition on Slag Foaming Under M'O Saturation and Fully Liquid Slag Conditions*

Slag foaming is strongly affected by the slag viscosity, which is dependent on the MgO content as well as basicity. The MgO content in M'O saturation slag, *i.e.*, $(\text{pct MgO})_{\text{M'O-sat.}}$, is dynamically affected by the operating conditions, and thus, the distribution of MgO in M'O saturation slag and fully liquid slag can be

Table I. Average Compositions of the Steel and EAF Slag for the Representative Slag Conditions (Mass Pct)

Slag Condition	Steel Composition				Slag Composition						
	C	Si	Mn	P	SiO_2	Al_2O_3	FeO	CaO	MgO	MnO	P_2O_5
Fully Liquid Slag (Type A)	0.14 (± 0.04)	0.2 (± 0.07)	0.9 (± 0.02)	0.02 (± 0.004)	17.4 (± 1.2)	15.7 (± 1.5)	24.6 (± 4.1)	24.7 (± 3.4)	7.5 (± 0.3)	9.9 (± 0.8)	0.18 (± 0.06)
M'O Saturation Slag* (Type B)	0.12 (± 0.02)	0.2 (± 0.04)	0.5 (± 0.03)	0.02 (± 0.005)	20.3 (± 1.5)	8.4 (± 0.7)	17.0 (± 3.9)	32.1 (± 2.9)	10.9 (± 1.2)	11.0 (± 0.5)	0.38 (± 0.06)

*Solid M'O fraction in slag ~ 5 mass pct (Calculated from FactSage™ 7.3).

evaluated by plotting (pct $MgO)_{M'O\text{-}sat.}$ as a function of slag basicity at 1843 K (1570 °C), as shown in Figure 7. The (pct $MgO)_{M'O\text{-}sat.}$, which was calculated using the FactSage™ 7.3 software, decreased with increasing basicity, indicating that MgO provides basic characteristics in the present slag. It is noteworthy that the MgO content in M'O saturation slag is clearly distributed beyond the (pct $MgO)_{M'O\text{-}sat.}$ limit but the MgO content in fully liquid slag is under the (pct $MgO)_{M'O\text{-}sat.}$ limit.

For slag composition beyond the M'O saturation limit, it is expected that slag viscosity is relatively higher than fully liquid slag due to the precipitation of solid compounds according to Einstein–Roscoe equation.[40] A higher viscosity increases the foaming index (Σ), which is equal to the retention or traveling time of gas in the slag, which can be used as a quantitative index of foam stability.[23,24] Hence, it is required to evaluate the effect of basicity on the foaming index. In the present study, the empirical equation of the foaming index of a multicomponent slag system proposed by Ito and Fruehan[24] was suggested by considering the thermophysical properties of slags as follows:

$$\sum = k\frac{\eta}{\sqrt{\rho \cdot \sigma}}, \qquad [11]$$

where k, η ρ, and σ are a constant, viscosity [Pa s], density [kg/m^{-3}], and surface tension [N/m], respectively. The constant k was assigned a value of 999 due to the value obtained from a similar slag composition by Kim *et al.*[28] Viscosity can be obtained by FactSage™ 7.3. Here, the effect of solid precipitation on slag viscosity is considered by using the Einstein–Roscoe equation. In addition, the density and surface tension are estimated using the polynomial expression by considering pure components, which are functions of temperature. Temperature dependencies of surface tension and density of slag components are available elsewhere.[22]

The foaming index of the present slag compositions as well as the previous reports by Fruehan *et al.*[23–27] are compared in Figure 8, which shows x-axis as CaO/SiO_2 (C/S) ratio as a basicity index due to original expression of the previous authors. The foaming index of the present study and Fruehan *et al.*'s data generally decreases with increasing basicity up to C/S = 1.0–1.2, depending on the slag composition, and it rebounds with increasing basicity, which is in excess of the liquidus composition. This behavior is strongly affected by the slag viscosity based on Eq. [11]. For slag basicity, $C/S < 1.2$, the viscosity decreases with increasing basicity but beyond 1.2, the viscosity that apparently increases with increasing basicity is affected by the precipitation of solid compounds, contributing to increase the foam stability.

Ito and Fruehan[23] reported that the precipitation of solid compounds like Ca_2SiO_4 has a larger effect than the increase of surface tension on foam stability. Hence, in the present slag system (CSFAMnM), the foaming index of M'O saturation slag is slightly higher than that of fully liquid slag. However, compared to the foaming index results of other researchers, the rate of change of

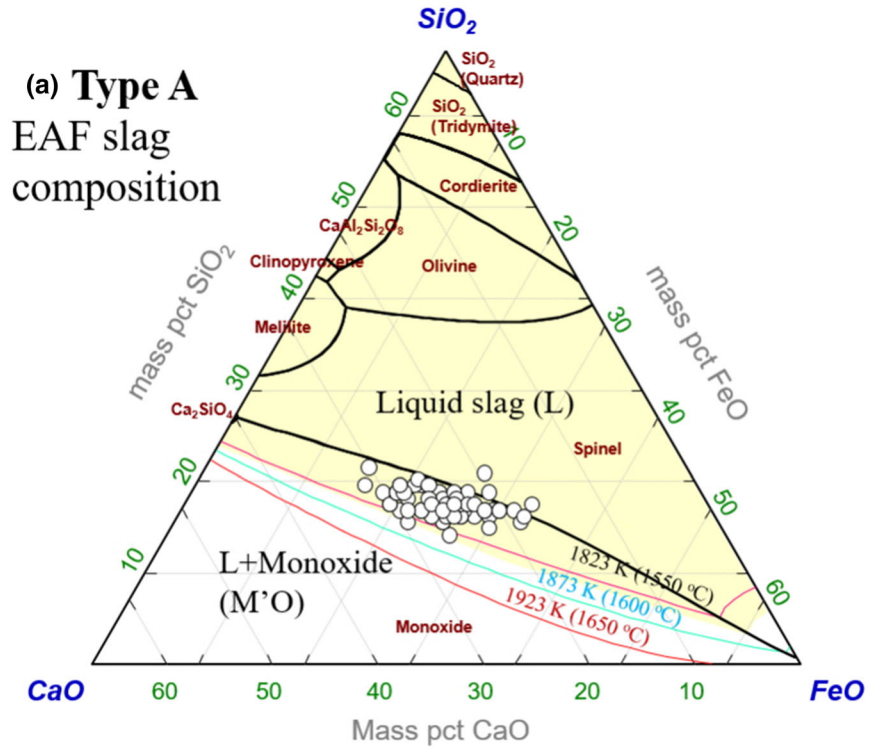

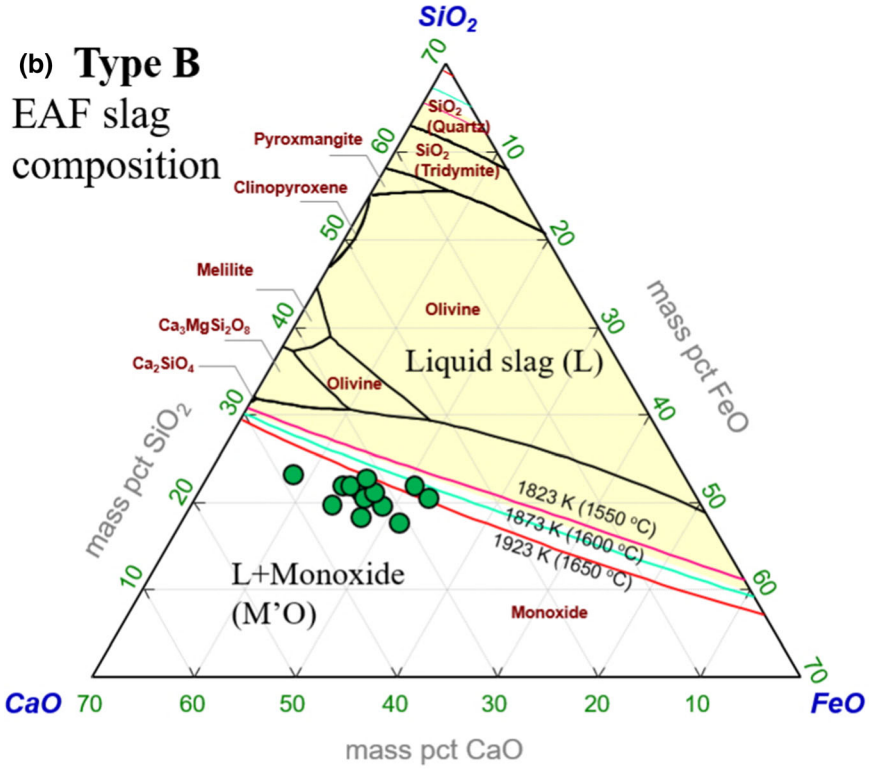

- L : Liquid slag
- Monoxide (M'O) : $(Fe,Mg,_{Mn})O$
- Olivine : $(Mg,Fe)_2SiO_4$
- Melilite : $Ca_2(Mg,_{Al,Fe})(Si,_{Al})_2O_7$
- Clinopyroxene : $CaMgSi_2O_6$
- Pyroxmangite : $(Mg,Mn)SiO_3$
- Cordierite : $(Mg,Fe)_2Al_4Si_5O_{18}$
- Spinel : $(Mg,Fe)Al_2O_4$

Fig. 1—EAF slag compositions in (*a*) the $CaO–SiO_2–FeO–8MgO–15Al_2O_3–10MnO$ system and (*b*) the $CaO–SiO_2–FeO–11MgO–8Al_2O_3–11MnO$ system in the temperature range from 1823 K to 1923 K (1550 °C to 1650 °C) and at $p(O_2) = 10^{-10}$ atm [Yellow region: liquid area at 1843 K (1570 °C)].

the present slag foaming varying with C/S ratio is not significant due to the higher temperature (1843 K [1570 °C]). Nonetheless, a comparison of foaming index between solid–liquid multiphase (M'O saturated) and fully liquid slags clearly provides that foaming index of M'O saturated slag is relatively higher than that of fully liquid slag. Specifically, the present results lead to introduce the efficient way for the enhanced foaming practice, contributing to actual improvement of a commercial plant operations.

Ito and Fruehan[23] studied the foaming of the $CaO–SiO_2–30FeO–3\sim5Al_2O_3$ (CSFA, mass pct) slag at 1573 K and 1673 K (1300 °C and 1400 °C). Because the temperatures (1573 K and 1673 K (1300 °C and 1400 °C)) are relatively lower than the present temperature (1843 K [1570 °C]), the value of the foaming index is basically higher and the downward concave shape is more remarkable. In other words, the decreasing rate (at $C/S < 1.2$) and increasing rate (at $C/S > 1.2$) with changing C/S ratio in Ito and Fruehan's results are significantly steeper than in the other results.

Jiang and Fruehan[25] studied foaming behavior of the $CaO–SiO_2–FeO–Al_2O_3$ (CSFA) and $CaO–SiO_2–MgO–Al_2O_3–FeO$ (CSMAF) slag at 1773 K (1500 °C) with $C/S > 1.0$. They reported that the foaming index decreases with a change of the FeO content because slag drainage from the foam becomes significant due to a decrease of viscosity. Compared to the present results, the temperature in the present study is higher than their experimental temperature and thus, the foaming index values of CSFA and CSMAF slag are slightly higher than that of the present CSFAMnM slag. Furthermore, the present slag contains relatively high FeO (10 to 30 pct) and MgO (to 10 pct) contents, contributing to the decrease of slag viscosity. Therefore, a combination effect of the slag composition and temperature affects the variation of the foaming index.

Even though the present data of the foaming index are insufficient with $C/S < 1.2$ region, it can be compared to the foaming index value reported by other researchers.[23–27] The foaming index of CSFA slag at 1573 K (1300 °C) reported by Ito and Fruehan[23] is not different from that of CSF slag at the same temperature reported by Jiang and Fruehan.[25] However, the foaming index of CSFM slag at 1713 K (1440 °C) reported by Jung and Fruehan[27] is much lower than CSF and CSFA slags at 1573 K and 1673 K (1300 °C and 1400 °C). Therefore, in order to obtain effective foam stability, it is necessary to control the temperature and slag composition simultaneously.

Various factors such as temperature, CaO/SiO_2 ratio, MgO content, and FeO also affect the formation of the M'O solid phase, which introduces foamy slag during the EAF process. Because the M'O phase mainly consists of MgO and FeO, it is required to understand the phase stability between MgO and FeO based on phase equilibria. Thus, to simultaneously consider MgO and FeO in molten slag, the stability diagram of the $CaO–SiO_2–FeO–MgO$ (C/S = 1.3 to 1.6) simplified slag system at 1843 K (1570 °C) and $p(O_2) = 10^{-10}$ atm is

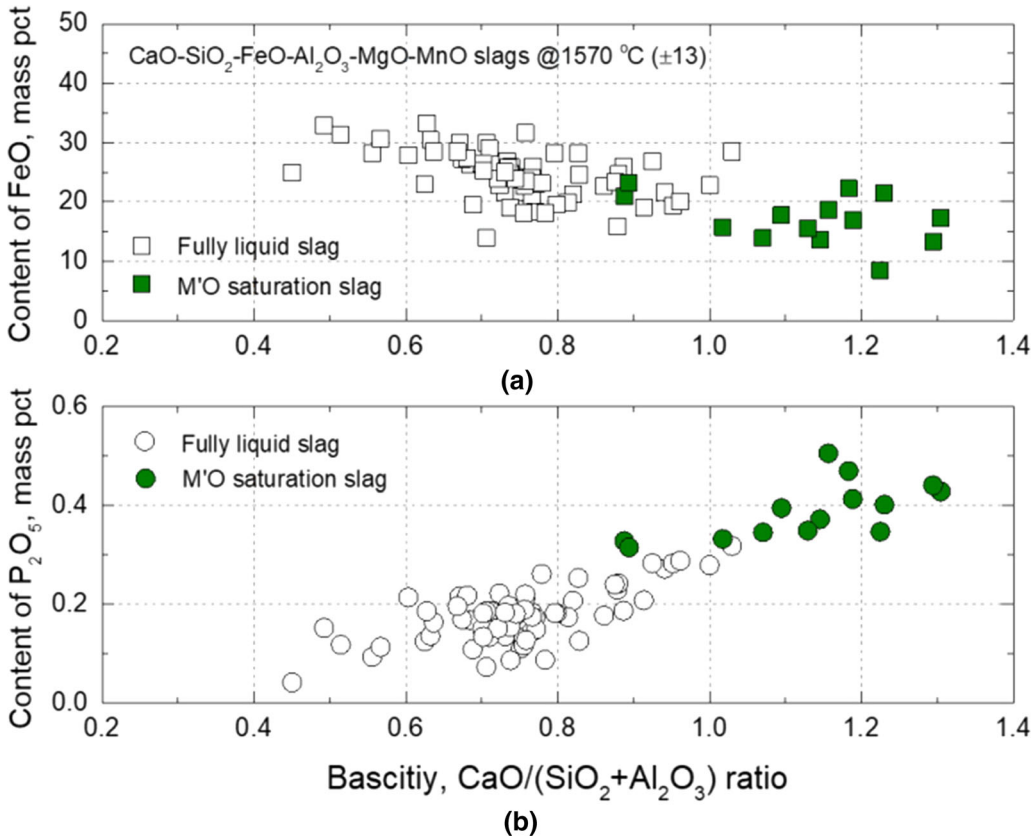

Fig. 2—Effect of basicity on the (*a*) FeO and (*b*) P_2O_5 contents in EAF slag under M'O saturation and fully liquid slag conditions.

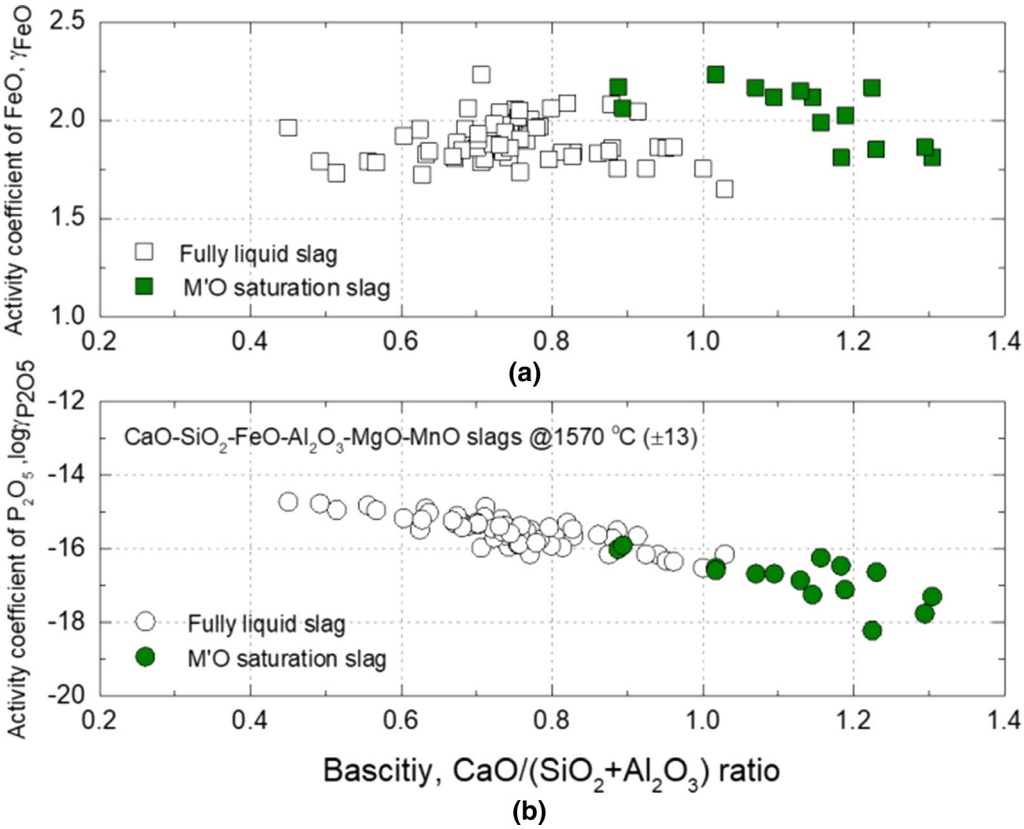

Fig. 3—Effect of basicity on the activity coefficients of (*a*) FeO and (*b*) P_2O_5 in EAF slag.

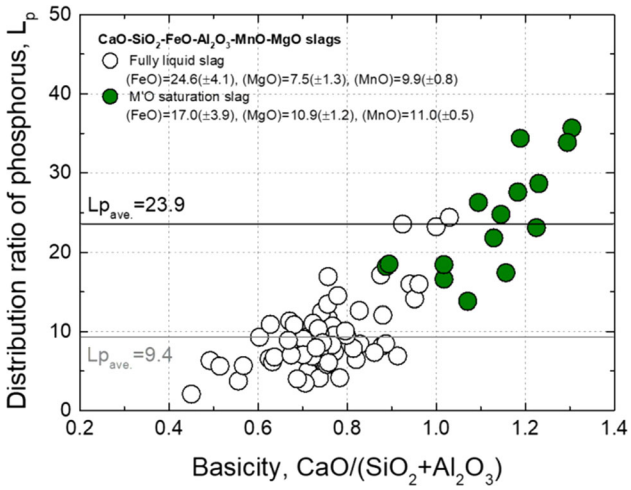

Fig. 4—Effect of basicity on the distribution ratio of phosphorus (L_P).

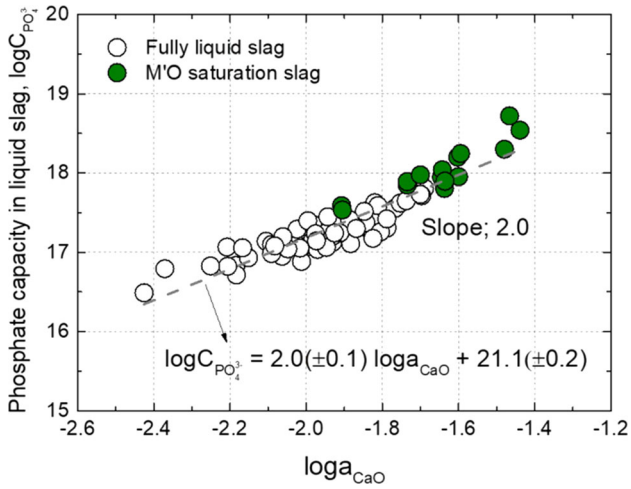

Fig. 5—Relationship between $\log C_{PO_4^{3-}}$ and $\log a_{CaO}$.

Table II. Interaction Parameters Used in the Present Study

e_P^i, $i \rightarrow$	Si	Mn	P	C
P	0.099	− 0.032	0.054	0.126

shown in Figure 9. Four regions of stable phases are extracted from the stability diagram: liquid (L), L + C_2S, L + (Fe,Mg)O, and L + (Fe,Mg)O + C_2S. Most slag composition in fully liquid slag was near the saturation limits of C_2S and (Fe,Mg)O based on the phase boundary at an average $C/S = 1.4$. However,

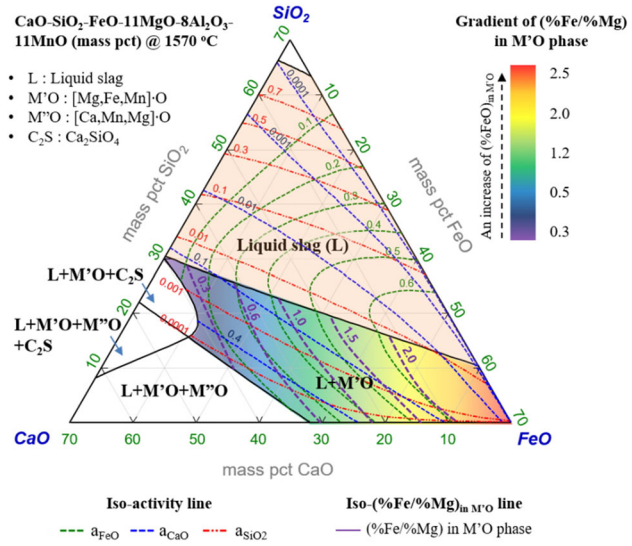

Fig. 6—Iso-activity contours of each oxide in the $CaO–SiO_2–FeO–11MgO–8Al_2O_3–11MnO$ phase diagram at 1570 °C and gradient of (pct Fe/pct Mg) in the M'O phase in the L + M'O region (Color figure online).

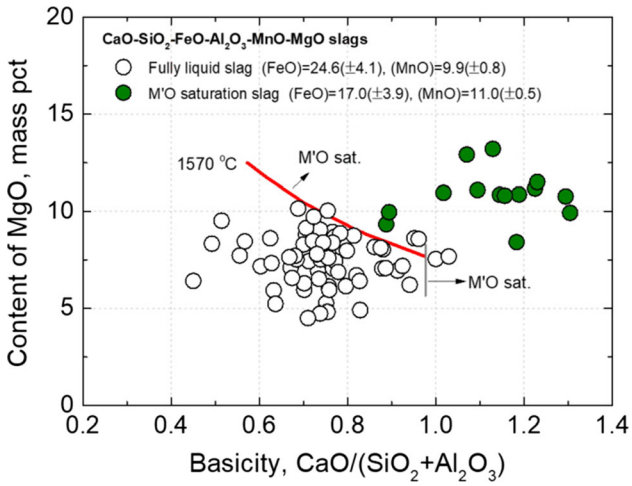

Fig. 7—Effect of basicity on the MgO content in fully liquid slag and M'O saturation slag.

M'O saturation slag was placed in the stable phase region, *i.e.*, L + (Fe,Mg)O + C_2S, based on the phase boundary at an average $C/S = 1.6$.

In particular, the dual saturation point of C_2S and (Fe,Mg)O is very important for effective slag foaming and dephosphorization during the EAF process.[22,26,29] The precipitation of (Fe,Mg)O can be explained by the activity of FeO (a_{FeO}) and MgO (a_{MgO}) in liquid slag. Iso-activity contours of FeO and MgO in the liquid phase at a fixed CaO/SiO_2 ratio of 1.4 are also shown in Figure 9. An increasing rate of a_{MgO} is more remarkable than a changing rate of a_{FeO} with a change of the slag composition. Namely, controlling the MgO content is more efficient than controlling the FeO content to saturate the (Fe,Mg)O phase. Thus, appropriate dolomite addition is necessary to form the (Mg,Fe)O phase as well as to prevent refractory corrosion.

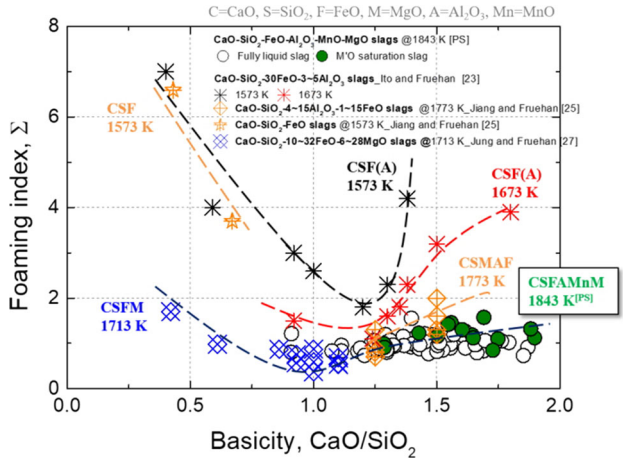

Fig. 8—Effect of CaO/SiO_2 ratio of slag and temperature on the foaming index (Σ).

The precipitation of C_2S in the EAF slag is closely related to both foam stability and dephosphorization. The precipitation of C_2S phase can be properly controlled by adding lime (CaO) and/or dolomite (CaO·MgO) fluxes. In particular, CaO addition is essential to refine molten steel by dephosphorization based on the thermodynamic discussions in Section III–A, but it is crucial to add the appropriate amount of CaO to prevent excess precipitation of C_2S. Pretorius and Carlisle[26] schematically depicted the relationship between the foaming index and the effective viscosity of slag. They reported that the foam stability and foam life are extended by increasing the residence time of the gas bubbles in the slag as an increase of the effective slag viscosity. However, slag becomes excessively oversaturated by precipitating excessive secondary particles and thus, the foaming index decreases.

It is known that phosphorus can be dissolved into the C_2S in slag by forming a dicalcium silicate and tricalcium phosphate ($3CaO·P_2O_5$) solid solution, *i.e.*, $C_2S–C_3P$ solution.[41–46] In other words, dephosphorization can be also performed by using solid C_2S in the slag. Ito *et al.*[43] confirmed that the distribution ratio of phosphorus $(L_P = (\text{pct C3P})_{\text{in C2S}}/(\text{pct C3P})_{\text{in slag}})$ between C_2S solid and molten $CaO–SiO_2–Fe_tO–P_2O_5$ slag at 1623 K to 1813 K (1350 °C to 1540 °C) was high, indicating that the stability of phosphorus as a $C_2S–C_3P$ solid solution is higher than that of molten slag. Similar research by Inoue and Suito[44] reported that the maximum distribution ratio of phosphorus $(L_P = (\text{pct } P_2O_5)_{\text{in C2S–C3P solution}}/(\text{pct } P_2O_5)_{\text{in slag}})$ between C_2S particles and $CaO–SiO_2–Fe_tO$ slag at 1573 K to 1833 K (1300 °C to 1560 °C) is obtained at the nose composition of the C_2S primary phase region in the $CaO–SiO_2–Fe_tO$ phase diagram. Furthermore, they proposed three reaction steps for phosphorus transfer from the $CaO–Fe_tO–P_2O_5$ slag. Namely, dephosphorization is possible even in solid-containing multiphase slag.[45,46]

Here, existence of solid compounds in molten slag directly affects slag foaming phenomena by changing the slag viscosity.[22,26,29] Slag foaming can indirectly induce an agitation effect which make it possible to improve dephosphorization kinetics. Mukawa and Mizukami[47] reported that the dephosphorization reaction rate is mixed controlled by mass transfer in the metal and slag phases. In their model calculation results, an increase of stirring energy promotes the dephosphorization reaction. Slag foaming leads to an increased suspension time of metal droplets compared to non-foamy slag.[48] Foamy slag will increase the reaction interface, contributing to enhance dephosphorization kinetics.[49] In addition, the stirring effect has an advantage by reducing the inhibition layer. Suito and Inoue[50] reported that dephosphorization by *mesoscopic* scale (several tens' micrometers in their claims) solid phase (CaO or C_2S) containing slag, called *meso-slag* (= multiphase slag), is inhibited by the protective layer formed at the meso-slag/metal interface if stirring is not employed. In other words, dephosphorization is dependent on agitation to reduce the inhibition layer. Hence, the agitation by slag foaming is expected to increase dephosphorization kinetics. From these previous studies, the solid–liquid multiphase slag with C_2S + M'O dual saturation by fluxing CaO and/or MgO will be more effective for higher dephosphorization as well as an efficient slag foaming practice. As a result, quantitative understanding of the effect of slag foaming on dephosphorization kinetics is vitally required in future work.

Because M'O saturation slag contains a proper amount of solid particles (approx. 5 mass pct on average in the present study), foamy slag is relatively obtained. Even though fully liquid slag is mainly placed in the liquid region, the slag nearly reaches the dual saturation point (Figure 9). It can be expected that a small amount of MgO by refractory corrosion will be dissolved into the molten slag to reach the (Fe,Mg)O saturation limit. In addition, if CaO can be additionally fluxed into the molten slag, the slag composition can be controlled to generate C_2S + M'O dual solid precipitation with high basicity. This will result in several advantages during the EAF process such as an increase of the thermodynamic driving force in liquid slag for dephosphorization, *viz*., CaO activity (a_{CaO}) and efficient slag foaming practice by an increase of the apparent viscosity.

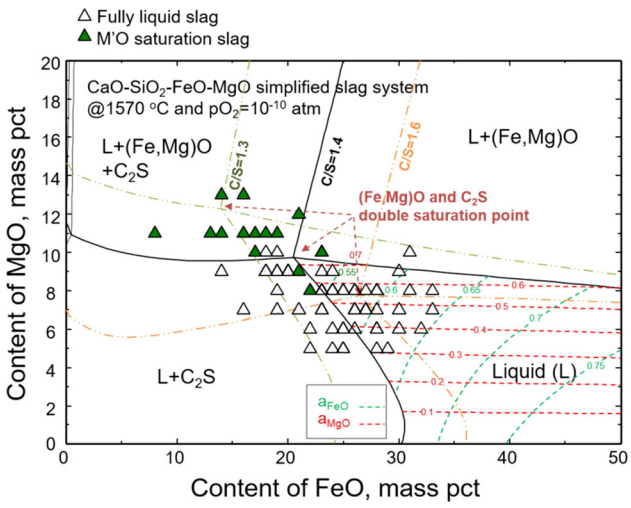

Fig. 9—Distribution of MgO and FeO in the simplified $CaO–SiO_2–FeO–MgO$ (C/S = 1.3 to 1.6) phase stability diagram at 1843 K (1570 °C) and $p(O_2) = 10^{-10}$ atm.

In summary, we thermodynamically evaluated the effect of slag composition at high basicity with solid–liquid multiphase slag with a small amount of M'O saturation (approx. 5 mass pct solid phase) on the dephosphorization of molten steel and slag foamability. It was confirmed that M'O saturation slag is more favorable for higher dephosphorization than fully liquid slag due to the high activity of CaO as a thermodynamic driving force. In view of foamability, the foaming index as a quantitative concept of slag foaming was clearly dependent on the temperature and slag composition. Moreover, foam stability was evaluated by applying a stability predominance diagram based on the phase equilibria. Consequently, based on the present findings, it can be suggested that efficient direction for dephosphorization and slag foaming during the EAF process is to generate basicity having high CaO activity with small amounts of M'O and C_2S solid compounds for dual saturation.

IV. CONCLUSIONS

The effect of the slag composition under M'O saturation and fully liquid conditions on dephosphorization and slag foamability was evaluated in EAF plant operation by considering physicochemical properties of slag and phase equilibria. Our major findings can be summarized as follows:

1. The thermodynamic behaviors of FeO and P_2O_5, which are strongly dependent on slag basicity, *i.e*., $CaO/(SiO_2 + Al_2O_3)$ ratio, can be understood by considering the activity coefficient of each oxide in EAF slag, irrespective of the slag conditions, *i.e*., M'O saturation and fully liquid slag. Namely, the stabilities of FeO and P_2O_5 are strongly dependent on the change of basicity as a thermodynamic driving force.
2. The distribution ratio of phosphorus (L_P) clearly increases with increasing basicity and the average L_P value in M'O saturation slag (L_P = 23.9) is about 2.5 times higher than in fully liquid slag (L_P = 9.4) due to higher CaO activity. The phosphate capacity ($C_{PO_4^{3-}}$) shows a good theoretical correlation with $CaO^{}$ activity on a logarithmic scale, indicating that the CaO activity as a good basicity index is a key parameter to increase dephosphorization efficiency.
3. The MgO content in M'O saturation slag, *i.e*., (pct $MgO)_{M'O\text{-}sat.}$ decreased with increasing basicity and the MgO content in M'O saturation slag is clearly distributed beyond the $(\%MgO)_{M'O\text{-}sat.}$ limit, while the MgO content in fully liquid slag is under the $(\%MgO)_{M'O\text{-}sat.}$ limit. Furthermore, the relationship between MgO and FeO at a fixed CaO/SiO_2 ratio was considered from the perspective of phase equilibria.

4. The change of the foaming index obtained in the present study and Fruehan *et al.*'s data generally decreases with increasing C/S ratio up to about 1.0–1.2 depending on the slag composition and it rebounds with increasing C/S ratio, which is in excess of the liquidus composition. This behavior is strongly affected by the slag viscosity. With $C/S < 1.2$, the viscosity decreases with increasing C/S ratio but beyond a C/S ratio of 1.2, the viscosity that apparently increases with increasing basicity is affected by the precipitation of solid compounds, contributing to increase foam stability. Therefore, a combinatorial effect of composition and temperature affects the variation of the foaming index.
5. Consequently, it can be suggested that an efficient direction for superior dephosphorization and slag foaming practice during the EAF process is to make basicity having high CaO activity with small amounts of M'O and C_2S dual phase saturation.

ACKNOWLEDGMENTS

This work was partly supported by the Korea Institute of Energy Technology Evaluation and Planning (KETEP, Grant Number 20212010100060), funded by the Ministry of Trade, Industry & Energy (MOTIE), Korea.

CONFLICT OF INTEREST On behalf of all authors, the corresponding author states that there is no conflict of interest.

REFERENCES

1. R.J. Fruehan: *The Making, Shaping, and Treating of Steel: Steelmaking and refining volume*. AISE Steel Foundation, 1998, pp. 597–622.
2. T.A. Bloom, D.R. Fosnacht, and D.M. Haezebrouck: *Iron Steelmak*., 1990, vol. 17, pp. 35–41.
3. N. Sano, W. Lu, P.V. Riboud, and M. Maeda: *Advanced Physical Chemistry for Process Metallurgy*, Academic Press, New York, 1997, pp. 45–56.
4. R.J. Fruehan and C.P. Manning: *AISI/DOE Technology Roadmap Program*, Final Report, Oct. 5, American Iron and Steel Institute, 2001.
5. J.H. Heo and J.H. Park: *Metall. Mater. Trans. B*, 2018, vol. 49B, pp. 3381–89.
6. M.K. Oh, T.S. Kim, and J.H. Park: *Metall. Mater. Trans. B*, 2018, vol. 51B, pp. 3028–38.
7. C. Chen, N. Wang, and M. Chen: *Steel Res. Int*., 2021, vol. 92, p. 2000719.
8. H. Suito, R. Inoue, and M. Takada: *Trans. Iron Steel Inst. Jpn*., 1981, vol. 21, pp. 250–59.
9. H. Suito and R. Inoue: *Trans. Iron Steel Inst. Jpn*., 1982, vol. 22, pp. 869–77.
10. H. Suito and R. Inoue: *Trans. Iron Steel Inst. Jpn*., 1984, vol. 24, pp. 47–53.
11. S. Nakamura, F. Tsukihashi, and N. Sano: *ISIJ Int*., 1993, vol. 33, pp. 53–58.
12. O.I. Ostrovski, Y.I. Utochkin, A.V. Pavlov, and R.A. Akberdin: *ISIJ Int*., 1994, vol. 34, pp. 849–51.
13. J. Im, K. Morita, and N. Sano: *ISIJ Int*., 1996, vol. 36, pp. 517–21.
14. J. Katsuki, Y. Yashima, T. Yamauchi, and M. Hasegawa: *ISIJ Int*., 1996, vol. 36, pp. S73–S76.
15. H. Ishii and R. Fruehan: *Iron Steelmak*., 1997, vol. 24, pp. 47–54.
16. T. Hamano and F. Tsukihashi: *ISIJ Int*., 2005, vol. 45, pp. 159–65.
17. C.M. Lee and R.J. Fruehan: *Ironmak. Steelmak*., 2005, vol. 32, pp. 503–08.
18. G. Li, T. Hamano, and F. Tsukihashi: *ISIJ Int*., 2005, vol. 45, pp. 12–18.
19. S. Basu, A.K. Lahiri, and S. Seetharaman: *Metall. Mater. Trans. B*, 2007, vol. 38B, pp. 357–66.
20. M.K. Cho, J.H. Park, and D.J. Min: *ISIJ Int*., 2010, vol. 50, pp. 324–26.
21. F. Li, X. Li, S. Yang, and Y. Zhang: *Metall. Mater. Trans. B*, 2017, vol. 48B, pp. 2367–78.
22. J.H. Heo and J.H. Park: *Metall. Mater. Trans. B*, 2019, vol. 50B, pp. 2959–68.
23. K. Ito and R.J. Fruehan: *Metall. Trans. B*, 1989, vol. 20B, pp. 509–14.
24. K. Ito and R.J. Fruehan: *Metall. Trans. B*, 1989, vol. 20B, pp. 515–21.
25. R. Jiang and R.J. Fruehan: *Metall. Mater. Trans. B*, 1991, vol. 22B, pp. 481–89.
26. E.B. Pretorius and R.C. Carlisle: *Iron Steelmak*., 1999, vol. 26, pp. 79–88.
27. S.M. Jung and R.J. Fruehan: *ISIJ Int*., 2000, vol. 40, pp. 348–55.
28. H.S. Kim, D.J. Min, and J.H. Park: *ISIJ Int*., 2001, vol. 41, pp. 317–24.
29. J. Bennett and K.S. Kwong: *Ironmak. Steelmak*., 2010, vol. 37, pp. 529–35.
30. R. Wang, B. Zhang, C. Hu, C. Liu, and M. Jiang: *Metall. Mater. Trans. B*, 2021, vol. 52B, pp. 1805–17.
31. J.S. Han, J.H. Heo, and J.H. Park: *Ceram. Int*., 2019, vol. 45, pp. 10481–91.
32. M.K. Oh and J.H. Park: *Ceram. Int*., 2021, vol. 47, pp. 20387–98.
33. S. Song, J. Zhao, and P.C. Pistorius: *Metall. Mater. Trans. B*, 2020, vol. 51B, pp. 891–97.
34. J.H. Park and D.J. Min: *Metall. Mater. Trans. B*, 1999, vol. 30B, pp. 689–94.
35. JH Park and DJ Min: *Metall. Mater. Trans. B*, 1999, vol. 30B, pp. 1045–1052.
36. J.H. Park and D.J. Min: *ISIJ Int*., 2004, vol. 44, pp. 223–28.
37. K.Y. Ko and J.H. Park: *Metall. Mater. Trans. B*, 2011, vol. 42B, pp. 1224–30.
38. M. Hino and K. Ito: *Thermodynamic Data For Steelmaking. The 19th Committee in Steelmaking*, The Japan Society for Promotion of Science, Tohoku University Press, 2010, pp. 259–64.
39. E.T. Turkdogan: *Physical Chemistry of High Temperature Technology*, Academic Press, New York, 1980, pp. 1–24.
40. R. Roscoe: *Br. J. App. Phys*., 1952, vol. 3, pp. 267–69.
41. R. Nurse, J. Welch, and W. Gutt: *J. Chem. Soc*., 1959, vol. 220, pp. 1077–83.
42. W. Fix, H. Heymann, and R. Heinke: *J. Am. Ceram. Soc*., 1969, vol. 52, pp. 346–47.
43. K. Ito, M. Yanagisawa, and N. Sano: *Tetsu-to-Hagane*, 1982, vol. 68, pp. 342–44.
44. R. Inoue and H. Suito: *ISIJ Int*., 2006, vol. 46, pp. 174–79.
45. S. Kitamura, H. Shibata, K. Shimauchi, and S. Saito: *Rev. Met. Paris*, 2008, vol. 105, pp. 263–71.
46. S. Kitamura, K. Miyamoto, H. Shibata, N. Maruoka, and M. Matsuo: *ISIJ Int*., 2009, vol. 49, pp. 1333–39.
47. S. Mukawa and Y. Mizukami: *ISIJ Int*., 1995, vol. 35, pp. 1374–80.
48. J. Martinsson, B. Glaser, and D. Sichen: *Metall. Mater. Trans. B*, 2016, vol. 47B, pp. 2710–13.
49. S. Khadhraoui, H. Odenthal, S. Das, M. Schlautmann, K. Hack, B. Glaser and R. Woolf: *La Metallurgia Italiana*, 2018, pp. 5–16.
50. H. Suito and R. Inoue: *ISIJ Int*., 2006, vol. 46, pp. 180–87.